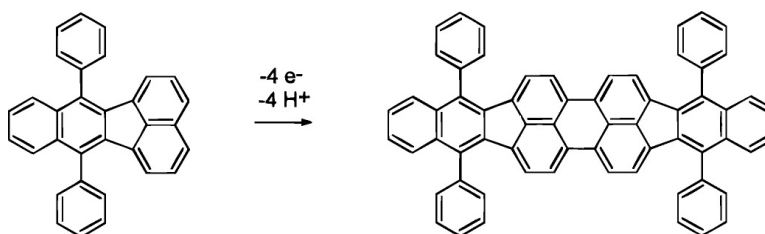


Anodic Coupling of Diphenylbenzo[*k*]fluoranthene: Mechanistic and Kinetic Studies Utilizing Cyclic Voltammetry and Electrogenerated Chemiluminescence

Jeff D. Debad, Jonathan C. Morris, Philip Magnus, and Allen J. Bard

J. Org. Chem., **1997**, 62 (3), 530-537 • DOI: 10.1021/jo961448e

Downloaded from <http://pubs.acs.org> on January 23, 2009



More About This Article

Additional resources and features associated with this article are available within the HTML version:

- Supporting Information
- Links to the 4 articles that cite this article, as of the time of this article download
- Access to high resolution figures
- Links to articles and content related to this article
- Copyright permission to reproduce figures and/or text from this article

[View the Full Text HTML](#)

Anodic Coupling of Diphenylbenzo[*k*]fluoranthene: Mechanistic and Kinetic Studies Utilizing Cyclic Voltammetry and Electrogenerated Chemiluminescence

Jeff D. Debad, Jonathan C. Morris, Philip Magnus,* and Allen J. Bard*

Department of Chemistry and Biochemistry, The University of Texas at Austin, Austin, Texas 78712

Received July 30, 1996[®]

Upon oxidation at a platinum electrode, (7,12-diphenyl)benzo[*k*]fluoranthene (**1**) undergoes intermolecular dehydrogenative coupling to form bis-4,4'-(7,12-diphenyl)benzo[*k*]fluoranthene (**2**). Further oxidation of this product results in a much slower intramolecular coupling reaction that yields dibenzo{[*l,l'*]-4,4',7,7'-tetraphenyl}diindeno[1,2,3-*cd*:1',2',3'-*lm*]perylene (**3**). **2** can be synthesized via bulk electrolysis of **1** and also by the chemical coupling of 4-bromo-7,12-diphenylbenzo[*k*]fluoranthene (**4**) with a nickel catalyst. Compounds **1–3** are capable of electrogenerated chemiluminescence (ECL), and their coupling reactions have been detected and followed using this technique. Cyclic voltammograms of **1** have been digitally simulated to provide mechanistic and kinetic insight into the initial intermolecular oxidative coupling reaction. Evidence supports an **EC₂EE** mechanism, in which the coupling of radical cations of **1** is the rate-limiting step. A second-order rate constant of $k = 7500 \text{ M}^{-1} \text{ s}^{-1}$ has been determined for the dimerization process by fitting experimental data to theoretical working curves.

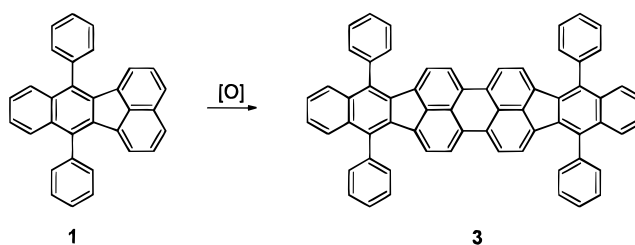
Introduction

Coupling reactions between organic radical cations have been widely used in organic synthesis, particularly in regard to biaryl bond formation.¹ These reactive ions are typically produced either electrochemically or with the use of strong oxidizing agents. A variety of such electrochemical reactions have been documented, including examples of both intramolecular, intermolecular, and cross-coupling reactions in both aliphatic and aromatic systems.² One of the major advantages of electrochemical methods over the use of chemical redox reagents is that electrochemistry allows superior control of the redox potential used for the reaction. In many cases, this can result in a more selective reaction and higher yields of desired products.

It is important to understand the mechanisms of these reactions not only from a fundamental perspective but also from a practical one, so that ideal reaction conditions can be employed to obtain optimum synthetic yields. If such reactions can be followed by spectroscopic or electrochemical techniques or a combination thereof, it may be possible to model the redox process mathematically. This could allow for the elucidation of the reaction mechanism along with the determination of kinetic rate constants.

We are interested in the possible decomposition pathways open to organic radical ions because stable ions are required for efficient electrogenerated chemiluminescence (ECL). ECL is typically produced by generating both the radical cation and radical anion of a compound at an electrode surface by pulsing the electrode potential between the oxidation and reduction potentials for the

Scheme 1



compound. The electron-transfer reaction that follows then produces excited states (R^*) that are capable of luminescence (eq 1).³ Recently, we reported the synthesis



and electrochemical properties of a large polycyclic aromatic hydrocarbon, dibenzo{[*l,l'*]-4,4',7,7'-tetraphenyl}-diindeno[1,2,3-*cd*:1',2',3'-*lm*]perylene (**3**, represented in the text as $\overline{R} \overline{R}$) (Scheme 1).⁴ This compound is formed when two (7,12-diphenyl)benzo[*k*]fluoranthene (**1**, RH_2) molecules are chemically coupled using oxidizing reagents such as CoF_3/TFA , $\text{AlCl}_3/\text{NaCl}$, and $\text{Ti}(\text{OCOCF}_3)_3$. Both starting material and product are capable of ECL, and we reported our preliminary investigations in this area.⁴ Blue or red light is observed at the electrode surface by employing compounds **1** or **3**, respectively, in a benzene/acetonitrile solvent mixture.

During these experiments we observed that the ECL spectrum of the monomer **1** also contained peaks similar in energy and intensity to those in the fluorescence spectrum of the dimer **3**. It was presumed that during the ECL experiment **3** was formed at the electrode surface via dehydrogenative coupling of the electrogenerated radical cations of **1** by analogy to the synthesis of

[®] Abstract published in *Advance ACS Abstracts*, January 15, 1997.

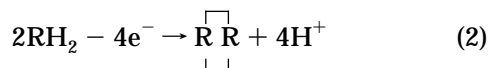
(1) (a) McKillop, A.; Turell, A. G.; Young, D. W.; Taylor, E. C. *J. Am. Chem. Soc.* **1980**, *102*, 6504. (b) Ebersson, L.; Hartshorn, M. P.; Persson, O. *J. Chem. Soc., Perkins Trans.* **2** **1995**, 409.

(2) See, for example: (a) Yoshida, K. *Electrooxidation in Organic Chemistry. The Role of Cation Radicals as Synthetic Intermediates*; John Wiley and Sons: New York, 1984. (b) Shono, T. *Electroorganic Synthesis*; Academic Press: London, 1991. (c) Kyriacou, D. *Modern Electroorganic Chemistry*; Springer-Verlag: Berlin, 1994.

(3) For reviews on ECL see: (a) Knight, A. W.; Greenway, G. M. *Analyst* **1994**, *119*, 879. (b) Faulkner, L. R.; Bard, A. J. In *Electroanalytical Chemistry*; Marcel Dekker: New York, 1977; Vol. 10, p 1.

(4) Debad, J. D.; Morris, J. C.; Lynch, V.; Magnus, P.; Bard, A. J. *J. Am. Chem. Soc.* **1996**, *118*, 2374.

3 using chemical oxidizing reagents. Because the product dimer could also be oxidized and reduced at the potentials used to produce ECL from **1**, red light from this dimer was visible along with the blue emission from the monomer. The conversion of **1** (RH₂) to **3** (R R) involves the removal of two electrons and two protons per molecule (eq 2). We were interested in the details of the reaction mechanism and the possibility of finding reaction intermediates.



Here we describe this radical cation coupling reaction in greater detail, including the observation, isolation, and independent synthesis of a stable reaction intermediate possessing only one bond between two monomer units (HR–RH). The electrochemical properties and ECL of this intermediate species are discussed. Cyclic voltammetry affords a convenient means to follow the oxidative coupling reaction, and we present a study of this process. Digital simulation of these voltammograms was carried out to establish the mechanism of the reaction and to determine the second-order rate constant of the dimerization process.

Experimental Section

Tetra-*n*-butylammonium hexafluorophosphate (TBAPF₆) (SACHEM, Inc.) was recrystallized from EtOH/H₂O (4:1) three times and dried at 100 °C before use. Benzene (Aldrich, ACS grade) and CH₃CN (Burdick and Jackson, UV grade) were used as received after being transported unopened into an inert atmosphere drybox (Vacuum Atmospheres Corp.). UV, fluorescence, electrochemical, and ECL solutions were prepared in a drybox and sealed in air-tight vessels for measurements completed outside the drybox.

¹H-NMR spectra were recorded on a General Electric QE-300 (300 MHz) spectrometer as solutions in deuteriochloroform (CDCl₃). Chemical shifts are expressed in parts per million (ppm, δ) downfield from tetramethylsilane (TMS) and are referenced to CDCl₃ (7.24 ppm) as internal standard. ¹³C-NMR spectra were recorded on a General Electric QE-300 (75 MHz) instrument as solutions in CDCl₃. Exact mass determinations were obtained on a VG analytical ZAB2-E instrument.

The relative fluorescence efficiency of **2** was measured⁵ using 5 μM solutions in benzene and with diphenylanthracene as a standard (λ_{exc} = 400 nm; φ_{DPA} = 0.98 in benzene⁶). Fluorescence spectra were recorded on a SLM Aminco SPF-500 spectrofluorometer, and UV spectra were recorded on a Milton Roy Spectronic 3000 array spectrophotometer.

ECL measurements were performed as previously reported⁷ using a charged couple device (CCD) camera (Photometrics CH260, Photometrics, Tucson, AZ) cooled to –130 °C. ECL solutions were similar in composition to those used for cyclic voltammetric measurements.

Cyclic voltammograms were recorded on a Bioanalytical Systems 100A electrochemical analyzer. The working electrode in all cases consisted of an inlaid platinum disk (1.3 mm diameter) that was polished on a felt pad with 0.05 μm alumina (Buehler, Ltd.) and sonicated in absolute EtOH for 1 min prior to each experiment. Platinum gauze served as a counter electrode. For standard cyclic voltammetric measurements, a silver wire was utilized as a quasi-reference electrode, and potentials were calibrated versus SCE by the addition of ferrocene as an internal standard using E°(Fc/Fc⁺) = 0.424 V vs SCE.

Voltammograms recorded for kinetic analysis utilized a Ag/Ag⁺ reference electrode (0.1 mM AgClO₄, 0.3 M TBAPF₆) separated from the bulk solution by a fine frit. This reference electrode was also calibrated by the addition of ferrocene following most experiments. Approximately 500 mg of activated alumina (ICN Biomedicals, Super I grade) was added to each solution used for kinetic measurements to scavenge any residual water. Data was gathered over a range of concentrations from 0.45 to 3.0 mM in **1** and over a range of scan rates from 75 to 17 000 mV/s.

Digital simulations were performed using Digisim 2.01 for Windows (Bioanalytical Systems, Inc.). All electron-transfer reactions were considered fast (k₀ = 10 000 s⁻¹), all disproportionations were assumed to be diffusion-controlled, and all α values were taken to be 0.5. The intermolecular coupling reactions were considered irreversible because of the following fast deprotonations and thus were assigned large equilibrium constants. Diffusion coefficients for **1** and **2** were measured using chronoamperometry,⁸ and ions were assigned the same coefficients as their neutral parents: 1.0 × 10⁻⁵ cm²/s for **1** and **1**⁺, and 5.0 × 10⁻⁶ cm²/s for **2**, **2**⁺, and **2**²⁺. Other parameters and the mechanisms used for the digital simulations are given in the text. Experimental cyclic voltammograms used for comparison to simulated voltammograms had the background current subtracted and were corrected for ohmic drop.

Bulk Electrolysis. Bulk electrolysis experiments were performed using a Princeton Applied Research Model 173/175 potentiostat/universal programmer. The working electrode consisted of a large platinum screen with a surface area of about 4 cm². A silver wire in a fritted compartment was used as a quasi-reference electrode (QRE). A platinum screen counter electrode was located in a compartment separated from the bulk solution by a fine frit.

In a typical experiment, **1** (15 mg), Na₂CO₃ (~300 mg), and alumina (~500 mg) were added to the working electrode compartment, and solvent containing electrolyte was added (benzene/acetonitrile 1:1; 0.1 M TBAPF₆). The potential of the working electrode was increased until a current of 1 mA began to flow and was then held at that potential. The reaction was deemed complete when a cyclic voltammogram of the reaction solution contained no waves attributable to **1**. Following electrolysis, the product was isolated by removing the solvent under vacuum and extracting with benzene. The extracts were filtered and the benzene removed under vacuum to leave a yellow solid that was then chromatographed on a silica column. Hexanes were used to elute any unreacted **1** (blue fluorescence) followed by CH₂Cl₂/hexanes (1:5) to remove the product, **2** (blue-green fluorescence, 24% yield).

Electrolyses of **2** and **3** were performed similarly, although in these cases the products were not isolated, but were identified by thin-layer chromatography.

4-Bromo-(7,12-diphenyl)benzo[*k*]fluoranthene (4). 1,3-Diphenylisobenzofuran (650 mg, 2.41 mmol) and 5-bromoacenaophthylene (555 mg, 2.40 mmol)⁹ in *p*-xylene (10 mL) were heated at reflux for 18 h, whereupon the xylene was removed by distillation. Anhydrous trifluoroacetic acid (1 mL) and dichloromethane (10 mL) were added, and the resulting mixture was heated at reflux for 18 h. Upon cooling, the solution was evaporated to dryness under vacuum to afford a brown solid. The solid was purified by chromatography over silica eluting with ethyl acetate/hexanes (1:10) to afford **4** (930 mg, 80%) as a yellow crystalline solid: mp 245–247 °C; ¹H NMR (300 MHz, CDCl₃) δ 6.37 (1H, d, *J* = 7.7 Hz), 6.60 (1H, d, *J* = 7.1 Hz), 7.34–7.43 (3H, m), 7.51–7.55 (5H, m), 7.60–7.68 (8H, m), 7.85 (1H, d, *J* = 8.3 Hz); ¹³C NMR (75.2 MHz, CDCl₃) δ 121.1 (C), 122.8 (CH), 125.1 (CH), 126.0 (2CH), 126.8 (CH), 126.9 (CH), 128.1 (CH), 129.3 (2CH), 129.8 (C), 129.9 (CH), 131.2 (CH), 133.3 (C), 133.9 (C), 134.2 (C), 135.1 (C), 135.2 (C), 136.4 (C), 136.6 (C), 136.9 (C), 138.5 (C); MS (CI) 484 (100), 482 (94); HRMS (CI) calcd for C₃₂H₁₉Br (M⁺) 482.0670, found 482.0658.

(8) Denuault, G.; Mirkin, M. V.; Bard, A. J. *J. Electroanal. Chem.* **1991**, *308*, 27.

(9) Mitchell, R. H.; Chaudhary, M.; Williams, R. V.; Flyes, R.; Gibson, J.; Ashwood-Smith, M. J.; Fry, A. J. *Can. J. Chem.* **1992**, *70*, 1015.

(5) Eaton, D. F. *Pure Appl. Chem.* **1988**, *60*, 1107.

(6) Morris, J. V.; Mahaney, M. A.; Huber, J. R. *J. Phys. Chem.* **1976**, *80*, 969.

(7) McCord, P.; Bard, A. J. *J. Electroanal. Chem.* **1991**, *318*, 91.

Bis-4,4'-(7,12-diphenyl)benzo[*k*]fluoranthene (2). Anhydrous nickel chloride (3 mg, 0.023 mmol), triphenylphosphine (42 mg, 0.16 mmol), zinc dust (60 mg, 0.945 mmol), and sodium bromide (70 mg, 0.68 mmol) in *N,N*-dimethylacetamide (1 mL) were heated at 80 °C until the solution become blood-red in color. Bromide **4** (100 mg, 0.207 mmol) in DMF/*N,N*-dimethylacetamide (1:1, 2 mL) was added in one portion, and the resultant green-gray fluorescent solution was heated at 80 °C for 18 h. Upon cooling, the solution was diluted with 2 N aqueous HCl solution and extracted with dichloromethane (3 × 50 mL). After the extracts were washed with water and saturated brine solution, they were dried (Na₂SO₄) and evaporated in vacuo to give a bright yellow solid. The solid was purified by chromatography over silica, eluting with hexanes to remove (7,12-diphenyl)benzo[*k*]fluoranthene (38 mg, 45%) followed by elution with dichloromethane/hexanes (1:5) to afford **2** (33 mg, 40%) as a yellow crystalline solid: mp 236–238 °C; ¹H NMR (300 MHz, CDCl₃) δ 6.59 (1H, d, *J* = 7.1 Hz), 6.70 (1H, d, *J* = 7.1 Hz), 7.16 (1H, t, *J* = 7.1 Hz), 7.31–7.42 (4H, m), 7.56–7.69 (12H, m); ¹³C NMR (75.2 MHz, CDCl₃) δ 127.9 (CH), 128.4 (CH), 131.4 (CH), 132.0 (CH), 133.0 (CH), 134.0 (CH), 134.1 (2CH), 135.4 (CH), 136.1 (CH), 139.1 (C), 140.6 (C), 141.0 (C), 141.07 (C), 141.14 (C), 141.8 (C), 142.5 (C), 142.7 (C), 142.8 (C), 145.0 (C); HRMS (CI) calcd for C₆₄H₃₈ (M⁺) 806.2973, found 806.2967.

Conversion of Bis-4,4'-(7,12-diphenyl)benzo[*k*]fluoranthene (2) to Dibenzotetraphenylperiflanthene (3). A mixture of bis-4,4'-(7,12-diphenyl)benzo[*k*]fluoranthene **2** (10 mg, 0.0124 mmol) and cobalt trifluoride (15 mg, 0.0129 mmol) in anhydrous trifluoroacetic acid (2 mL) was heated at reflux for 18 h. Upon cooling, the solution was diluted with dichloromethane (3 × 50 mL). After the dichloromethane extracts were washed with water and saturated brine solution, they were dried (Na₂SO₄) and evaporated in vacuo to give a black solid. The solid was purified by chromatography over neutral alumina, eluting with dichloromethane/hexanes (3:10) to give **3** (7 mg, 70%) as a purple-black solid, which was identical to that of an authentic sample.⁴

Results and Discussion

Electrochemistry. Bulk Electrolysis of 1. As mentioned above, the formation of **3** (R R) during the ECL of **1** (RH₂) was attributed to the coupling of electrogenerated radical cations **1**⁺. If this is indeed the case, then bulk oxidative electrolysis of the monomer **1** should form the same product and provide additional evidence for this dimerization scheme. The bulk electrolysis of **1** was thus carried out at a potential corresponding to the foot of the **1**/**1**⁺ wave in the compound's cyclic voltammogram (~+1.4 V vs SCE). At intervals, the reaction was halted and a voltammogram of the electrolysis solution was recorded to judge the extent of the reaction. The dimer **3** was not observed to form, although waves attributed to another product grew during the electrolysis with a concomitant decrease in the oxidation wave of the monomer.

The electrolysis product was isolated and identified as bis-4,4'-(7,12-diphenyl)benzo[*k*]fluoranthene (**2**, HR–RH), resulting from the formation of a single bond between two monomer units (Scheme 2). The position of the coupling in the reaction is not unexpected. Molecular orbital calculations on fluoranthene derivatives have shown that the HOMO has high electron density at the bond-forming site.¹⁰ To confirm the identity of this product, a chemical synthesis starting from the bromide **4** was carried out.¹¹ Dimerization of **4** proved to be



surprisingly difficult using the traditional Ullmann coupling.¹² However, the use of a Ni-based system¹³ proved successful and afforded a 40% yield of **2** (Scheme 2) along with the debrominated compound **1** in 45% yield.

Electrochemical Properties of 2. Although compound **2** was not observed during the chemical synthesis of the dimer **3** from the monomer **1**, the electrochemical experiments suggest that it is an intermediate in the transformation. Thus, further oxidation of **2** should result in a second dehydrogenative coupling to form **3**. The electrochemistry of **2** was investigated to study the stability of its cations and to obtain evidence for the expected cyclization reaction.

The cyclic voltammogram of **2** in benzene/acetonitrile solution is shown in Figure 1, along with those of **1** and **3** for comparison. The voltammogram of **2** contains two closely spaced oxidation waves at +1.34 and +1.49 V vs SCE that correspond to the formation of the radical cation and dication, respectively. The compound is also reduced to the dianion in two very closely spaced reductions centered around -1.75 V. The first reduction wave appears as a shoulder on the second, which is more clearly seen in the inset in Figure 1b. Typical values for the separation of first and second reduction or oxidation waves for polyaromatic hydrocarbons range from 400 to 700 mV,¹⁴ which is a much greater separation than observed here. The closer spacing found with **2** suggests that it is twisted about the central connecting bond such that full delocalization of the molecular orbitals over the entire molecule is not possible. Thus, oxidation or reduction leads to a localization of the charge on one end of the molecule, so that a second electron can be removed or added, respectively, to the other end more easily than would be expected for a fully delocalized and planar system. This is more obvious during the reduction of **2**, where the addition of a second electron occurs at nearly the same potential as the first.

Using the above arguments, the oxidation of **2** on a time scale consistent with scan rates above 200 mV/s (t₀

(12) Fanta, P. E. *Synthesis* **1974**, 9.

(13) Colon, I.; Kelsey, D. R. *J. Org. Chem.* **1986**, *51*, 2627 and references therein.

(14) (a) Peover, M. E. In *Electroanalytical Chemistry*; Bard, A. J., Ed.; Marcel Dekker: New York, 1967; Vol. 2, p 1. (b) VolSaji, T.; Aoyagui, S. *J. Electroanal. Chem.* **1983**, *144*, 143. (c) Jensen, B. S.; Parker, V. D. *J. Am. Chem. Soc.* **1975**, *97*, 5211. (d) Saji, T.; Aoyagui, S. *J. Electroanal. Chem.* **1979**, *98*, 163. (e) Chang, J.; Hercules, D. M.; Roe, D. K. *Electrochim. Acta* **1968**, *13*, 1197. (f) Bard, A. J. *Pure Appl. Chem.* **1971**, *25*, 379.

(10) Plummer, B. F.; Steffan, L. K.; Braley, T. L.; Reese, W. G.; Zych, K.; Van Dyke, G.; Tulley, B. *J. Am. Chem. Soc.* **1993**, *115*, 11542.

(11) See the Experimental Section for details on the preparation and characterization of this compound.

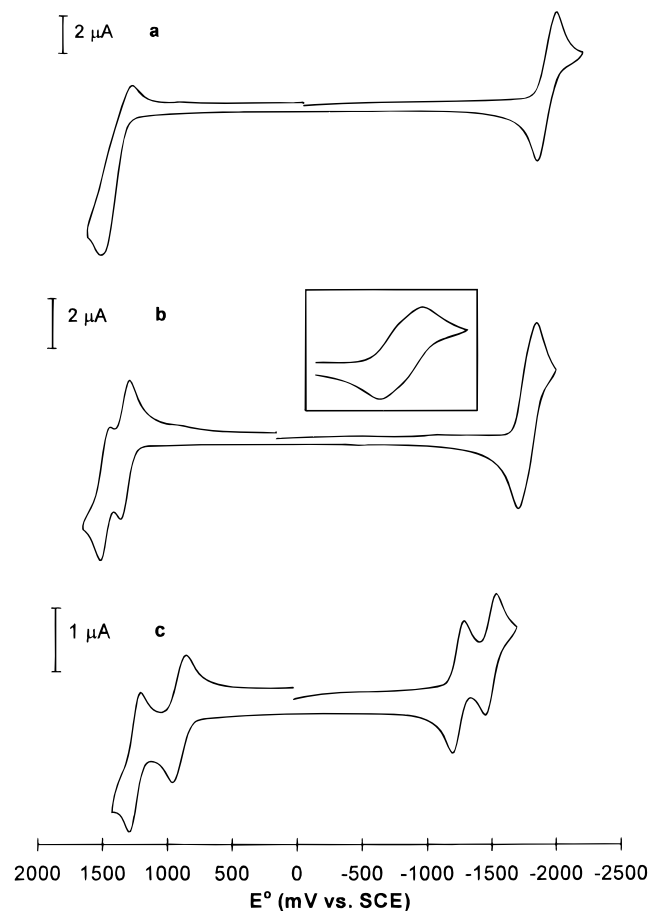


Figure 1. Cyclic voltammograms of (a) 1.5 mM **1**, (b) 0.56 mM **2**, and (c) 0.31 mM **3** in benzene/acetonitrile (1:1; 0.3 M TBAPF₆), scan rate 100 mV/s. The reduction wave of **2** is shown in the inset at a scale that more clearly illustrates the dual nature of the reduction.

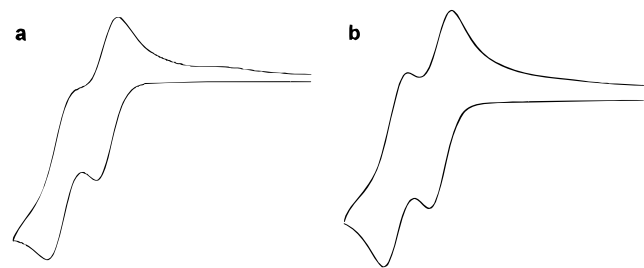
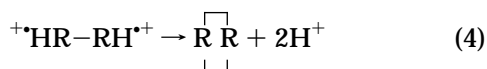


Figure 2. Cyclic voltammograms of the oxidation of **2** at (a) 50 mV/s and (b) 500 mV/s in benzene/acetonitrile (1:1; 0.3 M TBAPF₆).

≤ 100 ms) can be represented as



At slower scan rates the second oxidation wave becomes less reversible, demonstrating that the dication is unstable (Figure 2). In these slow-scan voltammograms, a new wave is observed on the return sweep at a potential matching that of the $3^{+}/3$ couple ($E^\circ = +0.95$ V vs SCE, Figure 1c). Thus, 2^{2+} undergoes a slow intramolecular coupling reaction to form the dimer **3** (see eq 4 and Scheme 2), which has been confirmed by bulk



oxidative electrolysis of **2**. In these experiments, **3** forms at potentials equal to or greater than that for the $2^{+}/2^{2+}$

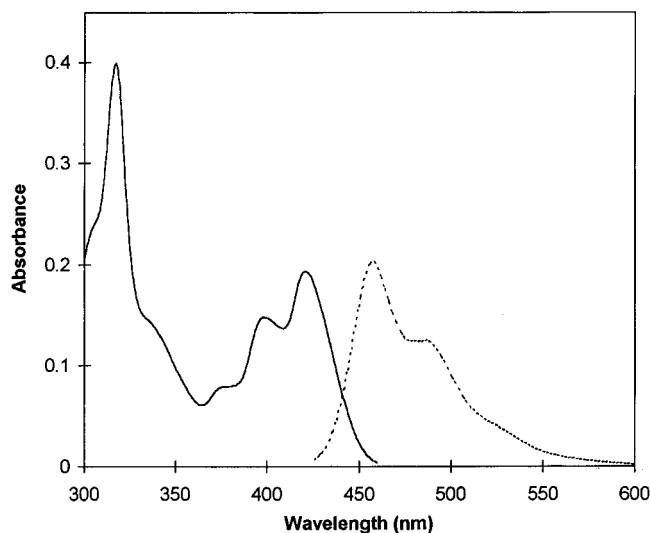


Figure 3. Absorption (—) and emission (---) spectra of a 5 μ M solution of **2** in benzene (1 cm pathlength; $\lambda_{\text{exc}} = 400$ nm).

couple, but not at potentials where only the radical cation is produced.

The synthesis of **2** from the monomer **1** via oxidation is an example where electrochemical methods are more suitable than chemical means. The applied potential used for the reaction needs to be carefully controlled to avoid oxidizing **2** to the dication and thereby initiating the intramolecular coupling to form **3**. There is only a 75 mV separation between the oxidation of the starting material and the formation of this dication, and it is difficult to obtain such selectivity with chemical reagents. Treatment of **1** with CoF₃/TFA or similar strong oxidizing agents forms **3** directly because these reagents are capable of oxidizing **2** to its dication. Chemical oxidation of **2** to **3** also occurs with CoF₃/TFA and results in a 70% yield of the red dimer.

Electrogenerated Chemiluminescence. We have previously described the ECL of monomer **1** and coupled product **3**.⁴ We also showed that the ECL spectrum seen during potential cycling of **1** shifted to longer wavelengths, signaling the formation of products (i.e., **2** and **3**).

Absorption and fluorescence spectra of the intermediate compound **2** are shown in Figure 3. Solutions of the molecule fluoresce in the blue-green region ($\lambda_{\text{max}} = 458$ and 484 nm) with a very high fluorescence efficiency, 0.95. The fluorescence spectrum is only red-shifted by 40 nm from that of the monomer that it is derived from ($\lambda_{\text{max}} = 418$ and 444 nm), again demonstrating the lack of delocalization across the single bond connecting the two parts of the molecule. A comparison to the fluorescence observed for **3** ($\lambda_{\text{max}} = 596$ and 646 nm) shows that the second C-C bond has the greater effect on emission properties due to the formation of a planar and now much more extended π system.

Its fluorescence and electrochemical properties indicate that **2** is a good candidate for electrogenerated chemiluminescence, since it has a high fluorescence efficiency and its cations and anions are accessible and fairly stable in a benzene/acetonitrile solvent system. Upon alternately forming the dication and dianion of **2** at an electrode immersed in a solution of the compound, blue-green light is produced at the electrode surface via an annihilation reaction analogous to eq 1. The ECL spectrum thus obtained is shown in Figure 4 for both stirred and

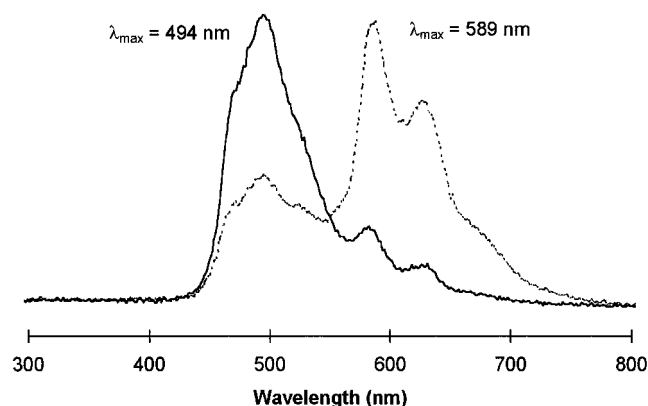


Figure 4. Electrogenenerated chemiluminescence of stirred (—) and unstirred (---) 0.24 mM solutions of **2** in benzene/acetonitrile (1:1; 0.3 M TBAPF₆; 1 Hz cycling between +1.55 and -1.80 mV).

unstirred solutions. The former is similar in energy to the compound's fluorescence spectrum if self-absorption of the lower wavelengths of the emission by the solution is taken into account. This similarity implies that the ECL emission also arises from the singlet state. The spectrum obtained from the unstirred solution is complicated and contains peaks that can be attributed to the ECL of **3**, which is formed when the dication of **2** undergoes intramolecular coupling. The potentials used in this experiment are more than sufficient to form anions and cations of **3**, and thus, this dimer also undergoes ECL once it forms. Emission from this product is not found with the stirred solution because the **3** formed is continuously swept away from the electrode.

Emission from **3** has also been observed during ECL experiments of **1**.⁴ In this case, however, ECL from **2** is also expected, since it is now known that **3** is formed via the intermediacy of this compound. ECL resulting from an unstirred solution of **1** does indeed show features attributable to the ECL of all three compounds: the blue-emitting monomer (**1**), the green intermediate (**2**), and the red dimer (**3**).

This system has, for the first time, allowed the analytical application of ECL for the determination of the products of electrode reactions. The formation of longer-wavelength emitting compounds has been reported in many ECL experiments; however, these products are typically reported as decomposition or oligomerization products and have not been isolated.¹⁵ We are now searching for further examples of such electrode reactions with the hopes of identifying their products utilizing ECL.

Kinetics and Mechanism from Cyclic Voltammetry and Digital Simulation

Cyclic Voltammetry of 1. The oxidation of **1** (RH₂) follows a complex path finally leading to oxidized **3** (R⁺R⁺), involving electron transfer, coupling, and deprotonation steps. The reaction, however, is extremely clean and provides the unique opportunity for studying the consecutive formation of two carbon-carbon bonds.

(15) (a) Werner, T. C.; Chang, J.; Hercules, D. M. *J. Am. Chem. Soc.* **1970**, *92*, 5560. (b) Fleet, B.; Keliher, P. N.; Kirkbright, G. F.; Pickford, C. J. *Analyst* **1969**, *94*, 847. (c) Werner, T. C.; Chang, J.; Hercules, D. M. *J. Am. Chem. Soc.* **1970**, *92*, 763.

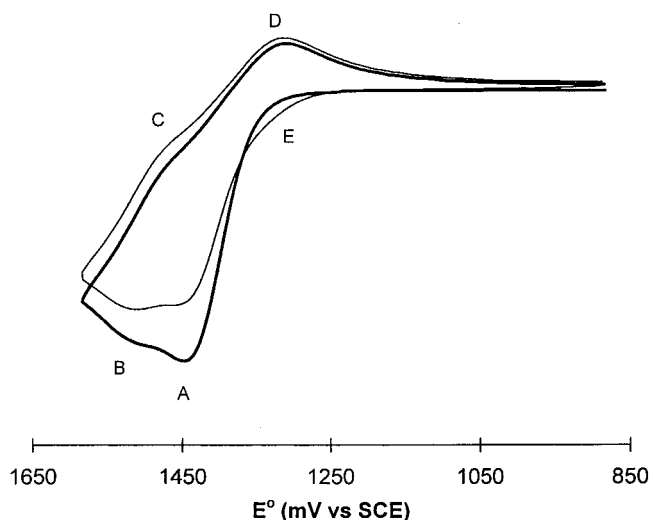


Figure 5. Cyclic voltammogram of 1.0 mM **1** in benzene/acetonitrile (1:1; 0.3 M TBAPF₆), scan rate 75 mV/s. A second scan recorded immediately following the first is plotted with a lighter line.

Table 1. Half-Wave Potentials for the Electron-Transfer Steps

reaction	<i>E</i> ^o (V vs SCE)
1 → 1 ^{•+} + e ⁻	1.419
2 → 2 ^{•+} + e ⁻	1.338
2 ^{•+} → 2 ²⁺ + e ⁻	1.492
3 → 3 ^{•+} + e ⁻	0.946
3 ^{•+} → 3 ²⁺ + e ⁻	1.290

Upon oxidation (indicated in the usual electrochemical notation as an **E** reaction¹⁶), **1** produces the radical cation that undergoes an intermolecular dehydrogenative coupling (C₂) to yield **2** (HR-RH). This intermediate is oxidized stepwise at nearly the same potentials to its dication (**EE**). This dication then undergoes an intramolecular dehydrogenative coupling (C) to form **3** (Scheme 2). This second coupling reaction is much slower than the first as judged by cyclic voltammetry. The **2**^{•+}/**2**²⁺ oxidation wave shows chemical reversibility above approximately 200 mV/s, while scans above 10 V/s are required to produce chemically reversible voltammograms of the **1**/**1**^{•+} couple. Species **3** is further oxidized at these potentials, in a stepwise reaction, to the dication (**EE**). Thus, the overall sequence from RH₂ to R⁺R⁺ can be described as an **EC₂EECEE** sequence (without separating the chemical deprotonation steps from the coupling reactions). Table 1 lists the half-wave potentials for the different electron-transfer steps.

A slow-scan (*v* = 75 mV/s) cyclic voltammogram of **1** is shown in Figure 5. The peak current for the oxidation wave is much greater than for a reversible one-electron reduction wave of the compound at this scan rate (Figure 1a). This is a result of the chemical reaction that follows oxidation of **1**, since the product that is formed, **2**, will also be oxidized at these potentials and result in the apparent removal of more than one electron from each molecule of **1** oxidized at the electrode. Thus, the first wave in the cyclic voltammogram (peak A in Figure 5) is a combination of the oxidation of **1** and the oxidation of **2** to **2**^{•+}.

A second wave (feature B) approximately 75 mV past the initial wave is due to the oxidation of the intermedi-

(16) Bard, A. J.; Faulkner, L. R. *Electrochemical Methods*; John Wiley and Sons: New York, 1980.

ate radical cation to its dication ($2^{+}/2^{2+}$). The reversibility of this couple at this scan rate is indicated both by the return peak for the process (feature C) and by the absence of a $3^{+}/3$ wave at less positive potentials on the return scan. Another feature is the lack of a return wave for the oxidation of the monomer ($1^{+}/1$) at this slow scan rate. Instead, a peak assigned to the reduction of the radical cation of the product is observed ($2^{+}/2$, peak D), indicating that most of the radical cations of **1** near the electrode are transformed into **2**. At higher scan rates the return wave for the oxidation of **1** is observed, since the rather slow chemical reaction does not consume all the 1^{+} generated on the forward sweep. A second scan recorded immediately after the first displays a shoulder on the monomer oxidation wave (feature E) showing the first oxidation wave of **2** formed during the first scan. Consistently, enhancement of the second oxidation wave of **2** (features B/C) is also observed in this second scan.

The oxidation of **1** can be followed by cyclic voltammetry over a range from irreversibility to reversibility, and this provides an opportunity to derive kinetic information about the initial coupling reaction. The intramolecular coupling of 2^{2+} to form **3** is relatively slow and is not important at scan rates above 75 mV/s. The following sections deal with the digital simulation of cyclic voltammograms of **1** to obtain mechanistic and kinetic information about the intermolecular coupling reaction.

Proposed Mechanisms. A number of mechanisms are available to explain the dimerization reaction that forms **2**, and all begin with the formation of 1^{+} at the electrode. It is assumed that this radical cation does not undergo deprotonation prior to reacting. If the radical underwent deprotonation, an oxidation wave that becomes reversible at much higher scan rates than the 10 V/s observed would be expected, because deprotonation reactions are typically very fast.¹⁷ If the solvent were to act as a deprotonating agent, this would result in pseudo-first-order kinetics, but this is not observed.

Second-order kinetics are assumed in the mechanism of the electrode process. This is based on two observations: the presence of dimerization products and the variation of the peak potential of the oxidation process with concentration of **1** in solution (Figure 6).

Two mechanistic possibilities need to be considered for radical cations reacting in a second-order process: radical cation–radical cation (rrc) coupling and radical cation–substrate coupling (rsc). Most reports^{17,18} of the oxidative coupling mechanisms of aromatic groups have reported radical–radical coupling; however, both mechanisms need to be appraised. Note the similarity between the intramolecular oxidative coupling reaction that produces **3** and the intermolecular coupling of radical cations of **1** being modeled here. The former reaction takes place only when the dication, and not the radical cation, of **2** is generated. If, as discussed above, the two positive charges are localized on either end of the molecule, then this reaction constitutes an example of a rrc mechanism. No coupling is observed upon formation of the radical cation 2^{+} , eliminating the possibility of an internal rrc mechanism in this case. This of course does not prove that the coupling to form **2** follows the same mechanism,

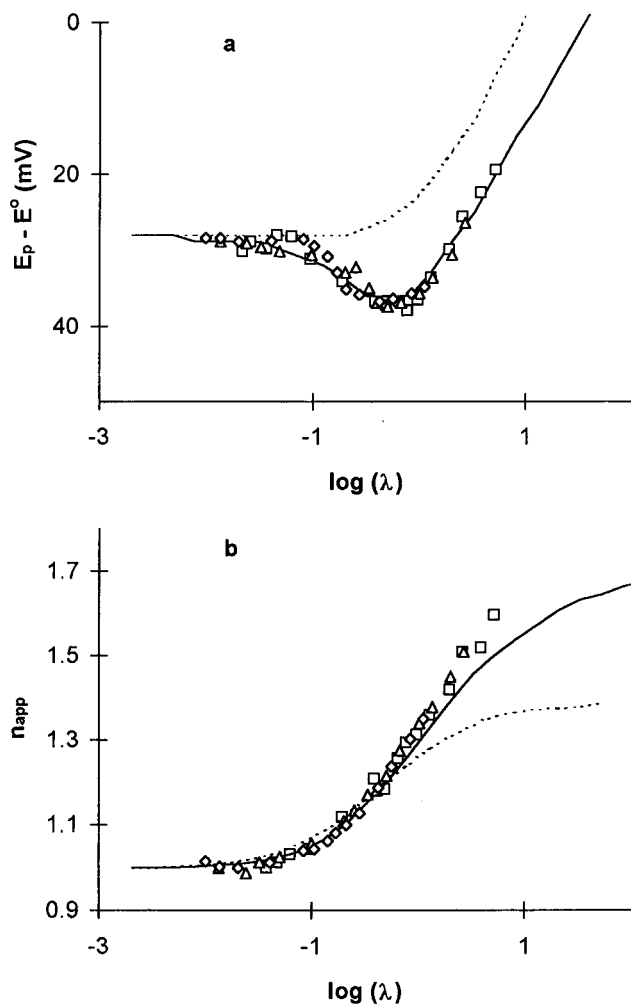
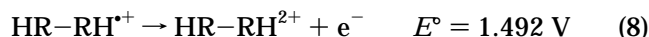
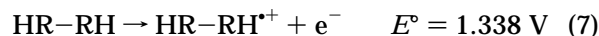
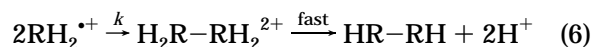


Figure 6. Theoretical working curves for rsc (---) and rrc (—) mechanisms ($\lambda = RTk_c/Fv$). Experimental data for 0.44 mM (\diamond), 1.04 mM (\triangle), and 2.00 mM (\square) concentrations of **1**; $k = 7500 \text{ M}^{-1} \text{ s}^{-1}$.

although this may be expected on the basis of the similarities of the two reactions.

The rrc mechanism is outlined in eqs 5–11. Once 1^{+} (RH_2^{+}) is formed, rate-limiting intermolecular dimerization with a concerted deprotonation forms **2** (HR-RH , eq 6). This product is then quickly oxidized to its radical



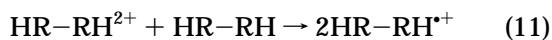
cation (HR-RH^{+}), since this reaction has an E° value more negative than the oxidation of the monomeric starting material (eq 7). 2^{+} is then oxidized to the dication (eq 8) at a potential 73 mV greater than for the oxidation of the monomer. This third electron transfer must be considered in modeling the cyclic voltammograms because its proximity to the initial oxidation wave will influence the peak current and potential of that wave. This series of reactions constitutes an EC_2EE process.

Because the three oxidations have different potentials, electron-transfer reactions that occur in solution also

(17) Yang, H.; Wipf, D. O.; Bard, A. J. *J. Electroanal. Chem.* **1992**, *331*, 913.

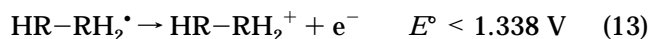
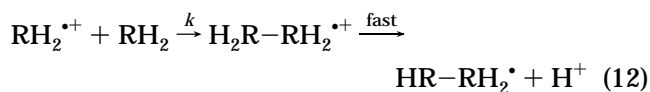
(18) For example, see: (a) Larumbe, D.; Gallardo, I.; Andrieux, C. P. *J. Electroanal. Chem.* **1991**, *304*, 241. (b) Yang, H.; Bard, A. J. *J. Electroanal. Chem.* **1991**, *306*, 87. (c) Marcoux, L. S.; Adams, R. N.; Feldberg, S. W. *J. Phys. Chem.* **1969**, *73*, 2611. (d) Nelson, R. F.; Feldberg, S. W. *J. Phys. Chem.* **1969**, *73*, 2623.

need to be considered. **2** can be oxidized by the monomer (eq 9), and the monomer can be oxidized by **2**^{•+} (eq 10) in separate reactions. The electron transfer between the



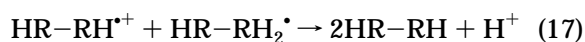
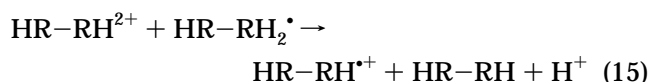
dicationic and neutral **2** is also thermodynamically favorable (eq 11). Equations 9–11 must be considered along with the heterogeneous electron-transfer reactions occurring at the electrode in modeling the oxidation process because the coupling reaction between radical cations of **1** is relatively slow. This results in the formation of **2** away from the electrode surface, where it is more likely to be oxidized by **1**^{•+} or **2**²⁺ than by the electrode.

Radical cation–substrate coupling would also result in second-order kinetics and would consist of reactions 5 and 12–17. Assuming deprotonation occurs concurrent to the intermolecular reaction between the radical cation and neutral monomer, the initial coupled species would be HR–RH₂[•] (eq 12). This intermediate species should then



undergo a fast oxidation at the electrode (eq 13) since its oxidation potential would be lower than that of **2** (HR–RH). Fast deprotonation of the product of this oxidation, HR–RH₂⁺ (eq 14), is required to satisfy the observed kinetics and results in an essentially irreversible electron-transfer reaction that can be modeled as a heterogeneous electron transfer followed by a fast chemical reaction (the deprotonation). As above, **2** will then undergo two separate oxidations (eqs 7 and 8), which leads to an EC₂ECEE mechanism for the rsc process.

Again, a number of electron-transfer reactions that are likely to occur in solution need to be considered (eqs 9–11 and 15–17). The required reactions are derived in a similar way as discussed above for the rrc mechanism, except that in this case additional reactions are needed due to the presence of the additional electroactive species, HR–RH₂[•] (eqs 15–17).



Digital Simulations. Digital simulations of the cyclic voltammograms for the oxidative process discussed above were performed as outlined in the Experimental Section. Theoretical working curves based on both the rrc and rsc mechanisms are plotted in Figure 6 using dimensionless parameters. The variation in peak potential is graphed using the difference between the peak potential and the oxidation potential of **1** ($E_p - E^\circ$). The dimensionless current function employed is the apparent number of

electrons transferred (n_{app}) and is calculated using the peak current at the highest scan rate as $n = 1$ for each concentration. $\text{Log}(\lambda)$, where $\lambda = RTkd/Fv$, is adopted as the ordinate variable¹⁹ (k is the second-order rate constant for the coupling reaction, c is the bulk concentration of the monomer, and v is scan rate in mV/s).

Experimental voltammograms were recorded for five different concentrations of **1** ranging from 0.44 to 2.0 mM and over scan rates from 75 to 17 000 mV/s. The points plotted in Figure 6 are the average results of two measurements taken at each scan rate and are corrected for ohmic drop. Plotted in a similar way to the theoretical working curves in Figure 6, these experimental data best matched the shape of the rrc working curve, and thus, the data were fit to this curve by varying the second-order rate constant, k . A sampling of the fitted experimental data are plotted in Figure 6 using $k = 7500 \text{ M}^{-1} \text{ s}^{-1}$, the average value found by fitting all the collected data to the rrc working curve. Further voltammograms were recorded for concentrations above 2 mM; however, these data displayed an increasing deviation from the working curves with increasing concentration. It thus appears that either another mechanism or side reactions begin to compete with radical–radical coupling at higher concentrations.

The slope of the $E_p - E^\circ$ vs $\text{log}(\lambda)$ working curve is typically used as a diagnostic tool in determining the mechanism of a reaction.²⁰ In this case, however, the second oxidation wave of the product interferes with the monomer oxidation wave, affecting its peak current and potential, and gives the rrc working curve a slope of 23 mV per decade in the kinetic-limited region. The experimental data, with a slope of 24 mV/decade, agree well with the working curve. If a similar working curve is generated without the interfering product oxidation, or with a much higher potential assigned to this oxidation so that it does not interfere with the initial peak, then the slope returns to the expected 20 mV.²⁰ The slope of the rsc curve in the kinetic-limited region is 42 mV and behaves in a similar fashion such that the slope of the simpler rsc mechanism is 30 mV/decade as expected.²⁰

A comparison between experimental and theoretical cyclic voltammograms is shown in Figure 7, with the simulations calculated using the rrc mechanism and $k = 7500 \text{ M}^{-1} \text{ s}^{-1}$. A slight increase in current is observed in the experimental voltammograms as compared to their simulated counterparts, especially at lower scan rates and at high potentials. This may be due to convection, electrode sphericity, or possibly to the onset of solvent oxidation. Nevertheless, the theoretical and experimental voltammograms match well over the concentration and scan rate ranges utilized in this study. The peak current and potentials are consistent with theory, and the experimental and simulated voltammograms have the same shape (Figure 6). The shape of the simulated voltammograms, particularly in the return sweep, is highly dependent on the parameters and mechanism used for the simulations. For example, if the solution electron-transfer reactions are not considered in the mechanisms, working curves similar to those in Figure 7 are calculated (although the dip is slightly less pronounced for the rrc curve); however, the shape of the voltammogram is quite different and does not fit the experimental data. Another example is the sensitivity

(19) Andrieux, C. P.; Savéant, J. M. In *Investigations of Rate and Mechanisms of Reactions Part II*; Bernasconi, C. F., Ed.; John Wiley and Sons: New York, 1986; Chapter VII.

(20) Nadjo, L.; Savéant, J. M. *J. Electroanal. Chem.* **1973**, *44*, 327.

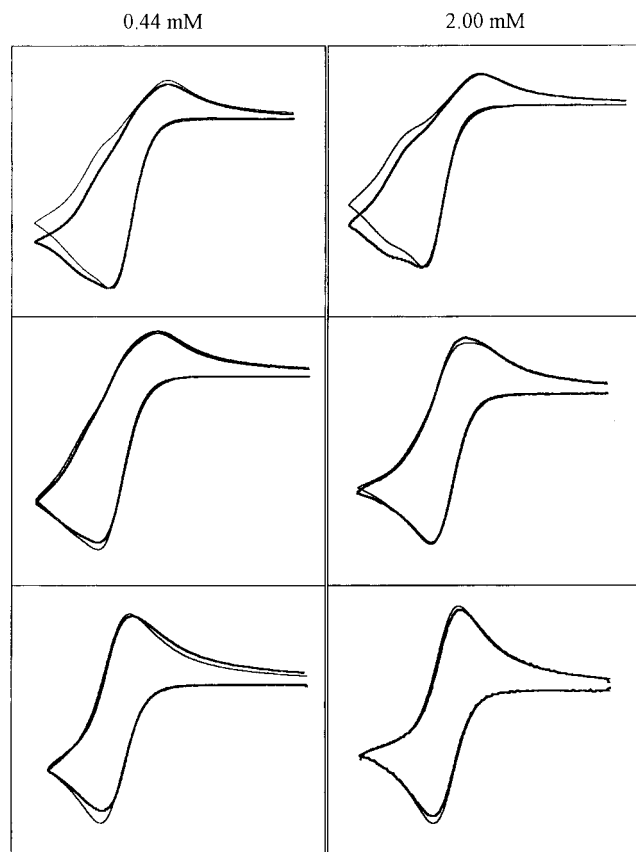


Figure 7. Comparison of selected experimental (darker lines) and simulated cyclic voltammograms for the oxidation of **1** (scan rate: top, 75 mV/s; middle, 800 mV/s; bottom, 17 000 mV/s). The rrc mechanism was used to generate the simulated voltammograms.

of the theoretical curves to the diffusion coefficients of the different species. Actual coefficients for all species were measured and used in the simulations because this method gave a much better fit to the experimental working curves and cyclic voltammograms than assigning a common coefficient to all the compounds involved.

On the basis of the excellent fit of the experimental data to the rrc working curves and the similar shape of the theoretical and experimental voltammograms, the

oxidation reaction that forms **2** from **1** is assumed to proceed by a radical cation–radical cation coupling mechanism.

Summary

Oxidation of (7,12-diphenyl)benzo[*k*]fluoranthene (**1**) at a platinum electrode leads to clean formation of bis-4,4'-(7,12-diphenyl)benzo[*k*]fluoranthene (**2**). Digital simulation of cyclic voltammetric data suggests that the reaction proceeds via an **EC₂EE** mechanism in which the rate-determining step is the dehydrogenative coupling of radical cations of **1**. The second-order rate constant for this dimerization process is 7500 M⁻¹ s⁻¹. The dication of **2** undergoes a much slower intramolecular dehydrogenative coupling reaction to yield dibenzo[*l,l'*-4,4',7,7'-tetraphenyl]diindeno[1,2,3-*cd*:1',2',3'-*lm*]perylene (**3**). The cyclic voltammetric data show that this latter coupling reaction only occurs upon formation of the dication and not the radical cation and may indicate that a similar radical cation–radical cation mechanism is operative here as well.

Electrolysis has been used to synthesize **2** from **1** and **3** from **2**. Although chemical oxidizing reagents are typically too strong to allow the direct synthesis of **2** from **1**, the coupling of a bromide derivative of **1** using a nickel catalyst forms **2** in good yield. Compounds **1–3** are all capable of electrogenerated chemiluminescence, and the ECL spectra of compound **1** also display emission from **2** and **3**. These compounds are formed near the electrode by the above coupling reactions upon generation of radical cations during the ECL experiment. This complex emission first alerted us to the nature of the reaction and initiated our investigation into these coupling processes.

Acknowledgment. The support of this research by the Texas Advanced Research Program (ARP-390), the National Science Foundation (CHE-9508525), and the Robert A. Welch Foundation is gratefully acknowledged. We thank the Natural Science and Engineering Research Council of Canada for their support in the form of a Postdoctoral Fellowship for J.D.D. We also thank Dr. Christophe Demaille for helpful discussions.

JO961448E